Effect of Spacer Length of Siloxane-Terminated Side Chains on Charge Transport in Isoindigo-Based Polymer Semiconductor Thin Films

*Jianguo Mei, Hung-Chin Wu, Ying Diao, Anthony Appleton, Hong Wang, Yan Zhou, Wen-Ya Lee, Tadanori Kurosawa, Wen-Chang Chen, and Zhenan Bao**

A series of isoindigo-based conjugated polymers (PII2F-C_mSi, m = 3–11) with alkyl siloxane-terminated side chains are prepared, in which the branching point is systematically "moved away" from the conjugated backbone by one carbon atom. To investigate the structure–property relationship, the polymer thin film is subsequently tested in top-contact field-effect transistors, and further characterized by both grazing incidence X-ray diffraction and atomic force microscopy. Hole mobilities over 1 $cm^2\ V^{-1}\ s^{-1}$ is exhibited for all soluble PII2F-C_mSi (m = 5–11) polymers, which is 10 times higher than the reference polymer with same polymer backbone. PII2F-C_9Si shows the highest mobility of 4.8 $cm^2\ V^{-1}\ s^{-1}$, even though PII2F-C_{11}Si exhibits the smallest π–π stacking distance at 3.379 Å. In specific, when the branching point is at, or beyond, the third carbon atoms, the contribution to charge transport arising from π–π stacking distance shortening becomes less significant. Other factors, such as thin-film microstructure, crystallinity, domain size, become more important in affecting the resulting device's charge transport.

1. Introduction

Charge transport properties of conjugated polymers have a profound impact on the performance of polymer-based organic electronics.[1–5] Many efforts to improve charge transport characteristics in polymer thin films include both materials design and processing optimization.[5–7] Recently, a large number of donor–acceptor conjugated polymers have demonstrated charge carrier mobilities over 1 $cm^2\ V^{-1}\ s^{-1}$, a benchmark value for the applications of conjugated polymers in flexible and printed electronics.[4,8,9] The predominant factor for this achievement is the rational development of a vast number of electron-rich and electron-poor building blocks. Polymer side chains have been recognized as a crucial component as they do not serve primarily as solubilizing groups to make polymers solution-processable, but also affect polymer packing motifs and film morphologies.[10,11] For example, regioregular and regiorandom poly(3-hexylthiophene)s are excellent examples, in which their side chain substitution pattern can result in a drastically different charge transport performance.[12,13] Conceivably, the type, shape, bulkiness, and length of side chains all impact the polymer physical properties and film morphologies. Indeed, side chain engineering has proven to be an effective tool for designing high-performance conjugated polymers.[9,14–18] We previously reported an effective strategy to facilitate π–π interaction and to enhance charge transport in donor–acceptor conjugated polymers by simply moving the branching point in side chains away from conjugated backbones.[19] From PII2T-Ref to PII2T-C_6Si (chemical structures are shown in **Figure 1**), the hole mobility increased fourfold from ≈0.6 to 2.5 $cm^2\ V^{-1}\ s^{-1}$ in thin-film transistors. Record high hole mobilities (up to 12 $cm^2\ V^{-1}\ s^{-1}$) in conjugated polymers have been recently achieved via a combination of the side chain engineering approach and careful choice of polymer backbone.[20] Pei, Yang, Oh, McCulloch and co-workers have all further investigated the influence of branching points on charge transport in IIDDT-C_m, PTDPPSe-SiC_m, PDPPTT-C_m (Figure 1).[16,20–23] These studies revealed the dependence of charge transport properties and thin-film morphologies on branching point positions.

Prof. J. Mei, H.-C. Wu, Prof. Y. Diao,
Dr. A. Appleton, H. Wang, Dr. Y. Zhou, Dr. W.-Y. Lee,
Dr. T. Kurosawa, Prof. Z. Bao
Department of Chemical Engineering
Stanford University
Stanford, CA 94305-5025, USA
E-mail: zbao@stanford.edu
Prof. J. Mei
Department of Chemistry
Purdue University
West Lafayette, IN 47907, USA
H.-C.Wu, Prof. W.-C.Chen
Department of Chemical Engineering
National Taiwan University
Taipei 10617, Taiwan
Prof. Y. Diao
Department of Chemical & Biomolecular Engineering
University of Illinois at Urbana–Champaign
600 South Mathews Avenue
Urbana, IL 61801, USA
H. Wang
Department of Chemistry
Tsinghua University
Beijing 100084, China

DOI: 10.1002/adfm.201500684

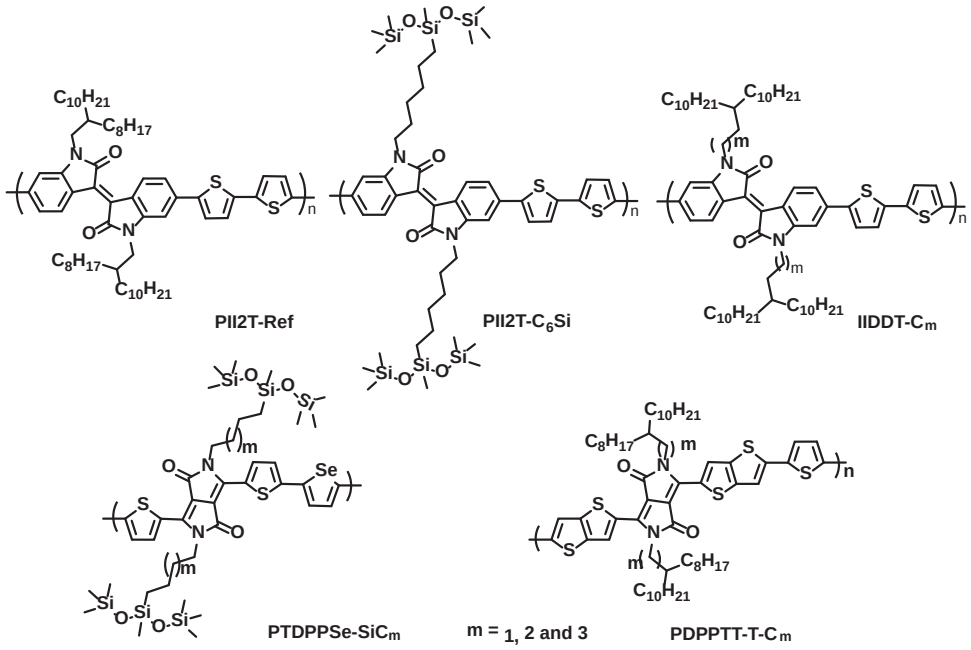

Figure 1. Chemical structures of side-chain engineered high performance conjugated polymers: PII2T-Ref and PII2T-C_6Si,[18] IIDDT-C_m,[22] PTDPPSe-SiC_m,[20] and PDPPTT-C_m. [23]

However, these studies only investigated a small number of polymers with a few carbon atoms between the backbone and the branching point. In this work, we perform a detailed and systematic study by moving the branching point one carbon at a time in the siloxane hybrid side chains, and proceeded to prepare a set of nine isoindigo-based conjugated polymers. We observed that seven of the nine polymers showed good solubility, i.e., C5–C11. Charge transport and thin-film morphology studies have been carried out on these soluble polymers. While preparing this manuscript, Pei and Kim published the studies on systematic investigation of side-chain branching position effect on electron carrier mobility in benzodifurandione-based poly(*p*-phenylene vinylene) (or BDPPV)[17] and hole carrier mobility in diketopyrrolopyrrole-selenophene vinylene selenophene (DPP-SVS) polymers[18] covering a spacer length of C1–C6 and C2–C9, respectively.

2. Results and Discussion

2.1. Monomer and Polymer Synthesis

The synthetic scheme of monomers and polymers is shown in **Scheme 1**. This synthetic sequence is similar to our previous report.[19] Briefly, N-alkylation of isoindigo core with commercially available n-bromo-1-alkene gave the isoindigo derivatives (IID-C_n, n = 1–9). During the purification by silica gel chromatography, we observed that the polarity of IID-C_n decreased upon increasing the spacer length. In other words, the retention time R_f values on thin-layer chromatography increased as the spacer lengths increased (Figure S1, Supporting Information). We attribute this phenomenon to the less molar mass ratio of polar isoindigo core in the side chains as the spacer lengths increase. The nine monomers (IID-C_mSi) were readily obtained by reacting alkene-functionalized isoindigo derivatives (IID-C_n) with 1,1,1,3,5,5,5-heptamethyltrisiloxane in the presence of Karstedt's catalyst, known as the hydrosilylation reaction. The solubility of the resulting IID-C_mSi is greatly enhanced. For example, IID-C_3Si can readily dissolve into hexane, while IID-C_n is barely soluble in hexane. Different from our previous study in using bi-thiophene co-monomer, we choose bi-furan as a co-monomer for polymerization in this study. The rationales are as follows: 1) the resulting polymers may have improved solubility, as have been reported for other furan-containing polymers,[24] 2) an even smaller π–π stacking distance may be obtained for these polymers, due to the smaller size of the oxygen atom in furan than the sulfur in the thiophene,[24,25] and 3) furan derivatives can be prepared from a variety of natural products and are considered to be renewable raw materials.[26] In comparison to the commonly used branched alkyl side chains,[17,18] our approach involves less synthetic steps to move the branching point in the hybrid siloxane side chains away from conjugated backbones. The obtained polymers (PII2F-C_mSi, m = 3–11), other than PII2F-C_4Si and PII2F-C_5Si, are soluble in chlorinated or aromatic solvents such as chloroform, chlorobenzene, and toluene. As expected, the solubility of the polymers increases with the spacer length. The soluble polymers (PII2F-C_mSi, m = 5–11) were purified by precipitation with acetone, filtered, washed with acetone, dried, and redissolved into hot chloroform. Palladium scavenger regent *N*,*N*-diethylphenylazothioformamide was added to remove catalyst residue. Reference polymer PII2F-Ref was also prepared for comparison,[27] in which the branching point is two carbon atoms away.

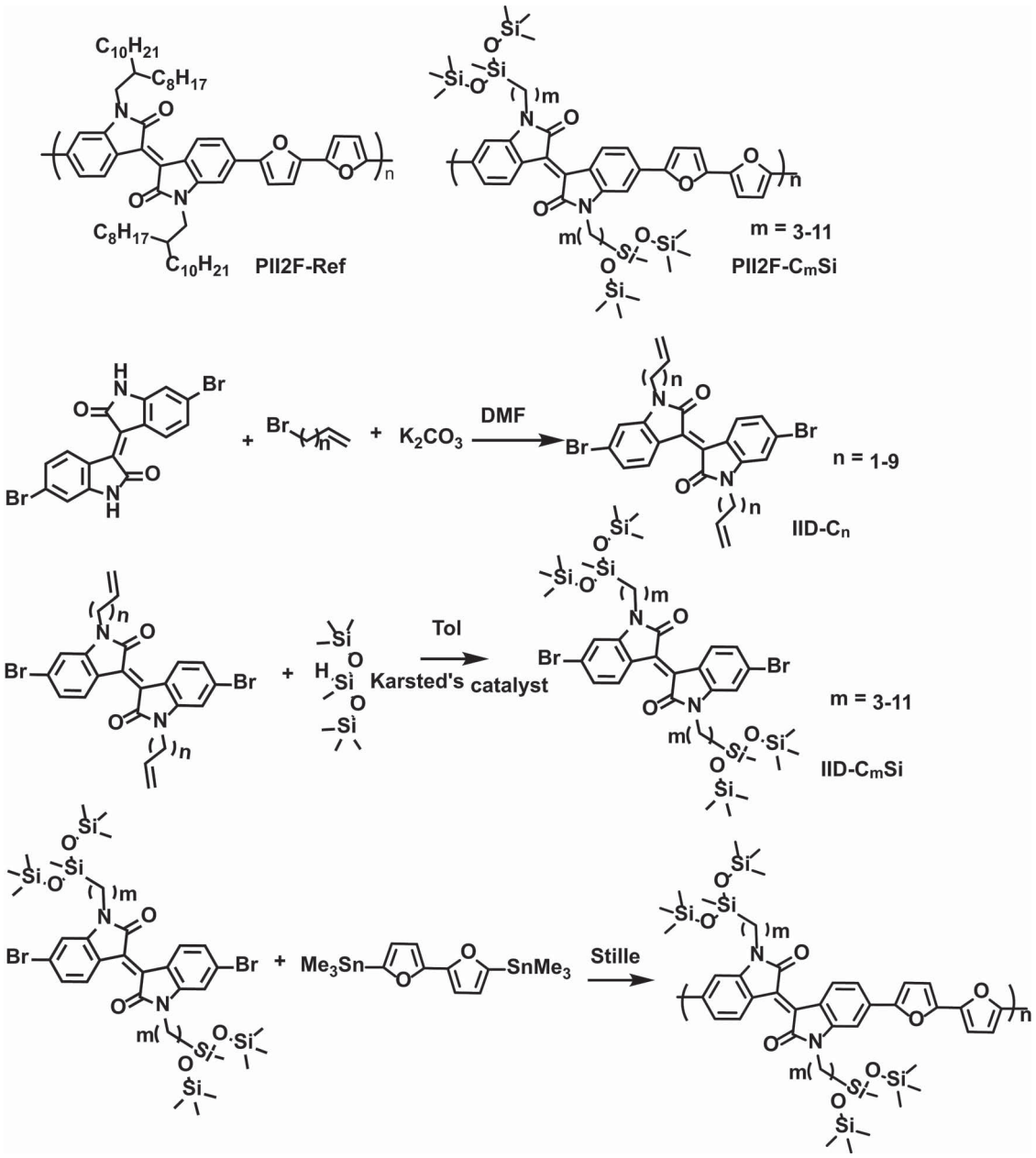

Scheme 1. Synthesis of PII2F-C_mSi (m = 3–11).

2.2. Characterization and Physical Properties

The soluble PII2F-C_mSi (m = 5–11) polymers were fully characterized by ^{1}H-NMR, gel-permeation chromatography (GPC), thermogravimetric analysis (TGA), differential scanning calorimetry (DSC), UV–vis spectroscopy, and photoelectron spectroscopy. **Table 1** summarizes some of the physical properties. Molecular weight and polydispersity were determined by gel permeation chromatography carried out in 1,2,4-trichlorobenzene at 200 °C. PII2F-C_mSi polymers have weight-averaged molecular weights in the range of 34–63 kDa with polydispersities of 1.4–2.1. Even though the GPC measurements were carried out under a high temperature, different degrees of aggregation may still exist in PII2F-C_mSi solutions. This renders the direct comparison of molecular weights challenging. PII2F-C_mSi polymers with short spacers are less soluble. More severe aggregations are thus likely to be present in their solutions. This may be a reason why PII2F-C_mSi polymers with short spacers gave higher molecular weights. Nevertheless, the high temperature GPC measurements suggest that all PII2F-C_mSi polymers are high molecular-weight polymers. TGA results reveal that these polymers have decomposition temperatures in the range of 390–420 °C. Interestingly, the shorter the spacer in the side chain, the higher the decomposition temperature was observed for the polymers. In comparison, the PII2F-Ref polymer showed a decomposition temperature of 379 °C.

Table 1. Physical properties of PII2F-C_mSi and PII2F-Ref.

Polymer	M_w[a)] [kDa]	PDI [–]	T_d [°C]	HOMO [eV]
PII2F-C_4Si	51.8	1.97	418	–5.25
PII2F-C_5Si	54.7	1.58	404	–5.35
PII2F-C_6Si	50.4	1.74	401	–5.30
PII2F-C_7Si	56.2	1.91	405	–5.25
PII2F-C_8Si	63.2	1.81	403	–5.25
PII2F-C_9Si	48.3	2.10	399	–5.25
PII2F-C_{10}Si	34.1	1.37	397	–5.25
PII2F-C_{11}Si	34.0	1.42	391	–5.35
PII2F-Ref	55.9	2.08	379	–5.32[27]

[a)]Molecular weight was determined by gel permeation chromatography carried out in 1,2,4-trichlorobenzene at 200 °C; decomposition temperature was determined by thermogravimetric analysis; energy level (HOMO) was estimated by photoelectron spectroscopy (PES).

DSC did not reveal any noticeable phase transitions between –50 and 300 °C for all the polymers. Grazing incidence X-ray diffraction (GIXD) studies show that PII2F-C_mSi polymer films are semicrystalline. More details are presented in the next section. All the PII2F-C_mSi polymers have nearly identical solid-state UV–vis absorption spectra (Figure S2, Supporting Information), with an absorption onset at around 773 nm. The highest occupied molecular orbital (HOMO) levels for the polymers are in the range of –5.25 and –5.35 eV, estimated by photoelectron spectroscopy.

2.3. Polymer Field-Effect Transistors (FETs) Characteristics

To investigate the relationship between the side chain spacer length and the thin film charge transport characteristics, bottom-gate/top-contact FET devices were fabricated. The 300 nm thick SiO_2 dielectric layer of highly n-doped silicon substrate was modified with a dense crystalline octadecyltrimethoxysilane (OTS) self-assembly monolayer to enhance the electrical performance using our previous reported procedure.[28] P-channel transfer and output characteristics are depicted in **Figure 2** and the device performance parameters are summarized in **Table 2**. For the as-prepared devices without thermal annealing, average p-channel mobilities were obtained in a range of 0.9–1.7 $cm^2\ V^{-1}\ s^{-1}$ with on/off current ratio of 10^5–10^6. These values are much higher than the PII2F-Ref polymer device (0.1 $cm^2\ V^{-1}\ s^{-1}$). Annealing at 200 °C greatly improves the charge transport characteristics. The mobilities of annealed devices are up to 3 $cm^2\ V^{-1}\ s^{-1}$, with high on/off current ratios (10^5–10^6). The large V_{th} of the studied FETs may attribute to the large bias stress, contact resistance from source/drain contacts and active layer, or low capacitance of the SiO_2 dielectric layer during the measurement. Among these siloxane-terminated polymers, PII2F-C_9Si exhibited the highest mobility of 3.4 $cm^2\ V^{-1}\ s^{-1}$. The use of mixed-solvent chloroform/chlorobenzene (9/1, v/v) further improved its charge transport characteristics of PII2F-C_9Si (see Figure S3, Supporting Information). A maximum mobility up to 4.8 $cm^2\ V^{-1}\ s^{-1}$ was obtained for the devices annealed at 200 °C. This value is substantially higher than that of PII2T-C_6Si (2.48 $cm^2\ V^{-1}\ s^{-1}$) in our previous work.[19] Note that PII2F-C_6Si also shows a higher mobility (3.2 $cm^2\ V^{-1}\ s^{-1}$) compared to PII2T-C_6Si. Moreover, the FET characteristics, including mobility, on/off current ratio, and threshold voltages, did not show obvious sign of degradation (Figure S4, Supporting Information), while the devices were stored and tested under ambient environment for around 1 month (relative humidity ≈40–50%).

2.4. Morphological Characterizations

To probe the thin film morphologies as the length of the side chain varies, grazing incidance X-ray diffraction (GIXD) was used to characterize the thin films that were deposited onto OTS-modified Si substrates. GIXD reveals the evolution of several morphological characteristics as the siloxane chain length varies: lamellar spacing, π–π stacking distance, degree of crystallinity, and out-of-plane orientation distribution of crystallites (**Table 3**, **Figure 3**). First, as expected, the lamellar spacing of PII2F-C_mSi polymers increased with the spacer length. At the same time, the π–π stacking distances decreased progressively as the length of siloxane side chain increases, by up to ≈1% from C5 to C11. This observation can be attributed to the steric hindrance imposed by the siloxane groups, preventing the close stacking of the II2F cores. However, the effect is gradually lessened as the spacer length increases. In particular, the PII2F-C_{11}Si exhibited a π–π stacking distance of 3.38 Å, the smallest observed in conjugated polymers.[29] The decreased π–π stacking distance is expected to have a positive impact on the charge carrier mobility, as we have shown in our previous work.[19] In addition to the decreased π–π stacking distance, we also observed that crystalline domain coherence length along the in-plane direction was improved from C5 to C11, as indicated by the decrease in the full width at half maximum (FWHM) of the π–π stacking peak (Table 3). This trend, again, is expected to facilitate interchain charge transport in the polymer thin films.[30]

The out-of-plane orientation distribution of crystallites, on the other hand, shows a nonmonotonic trend, as evidenced by both the lamella peaks (e.g., (200) and (300)) and the π–π stacking peak, (010). A shown in Figure 3, all PII2F-C_mSi thin films exhibited a bimodal distribution of out-of-plane orientations, and both face-on and edge-on populations of crystallites were observed for conjugated backbones. In particular, going from C5 to C9, the face-on population decreased relative to the edge-on population, judged from the fact that the face-on portion of the (010) ring lost some intensity, whereas the edge-on (010) portion increased in intensity. This transition was also evident from the lamella peaks. The morphology of highly oriented, edge-on crystallites is favorable for in-plane intermolecular charge transport. However, when the spacer length went from C9 to C11, the face-on crystallites became far less oriented out-of-plane as indicated by the wide angular spread of the lamella peaks (e.g., (200), (300)). Putting all the above morphological observations together, we can explain why PII2F-C_9Si possesses a favorable morphology to facilitate in-plane charge transport. Decreasing spacer length to below C9

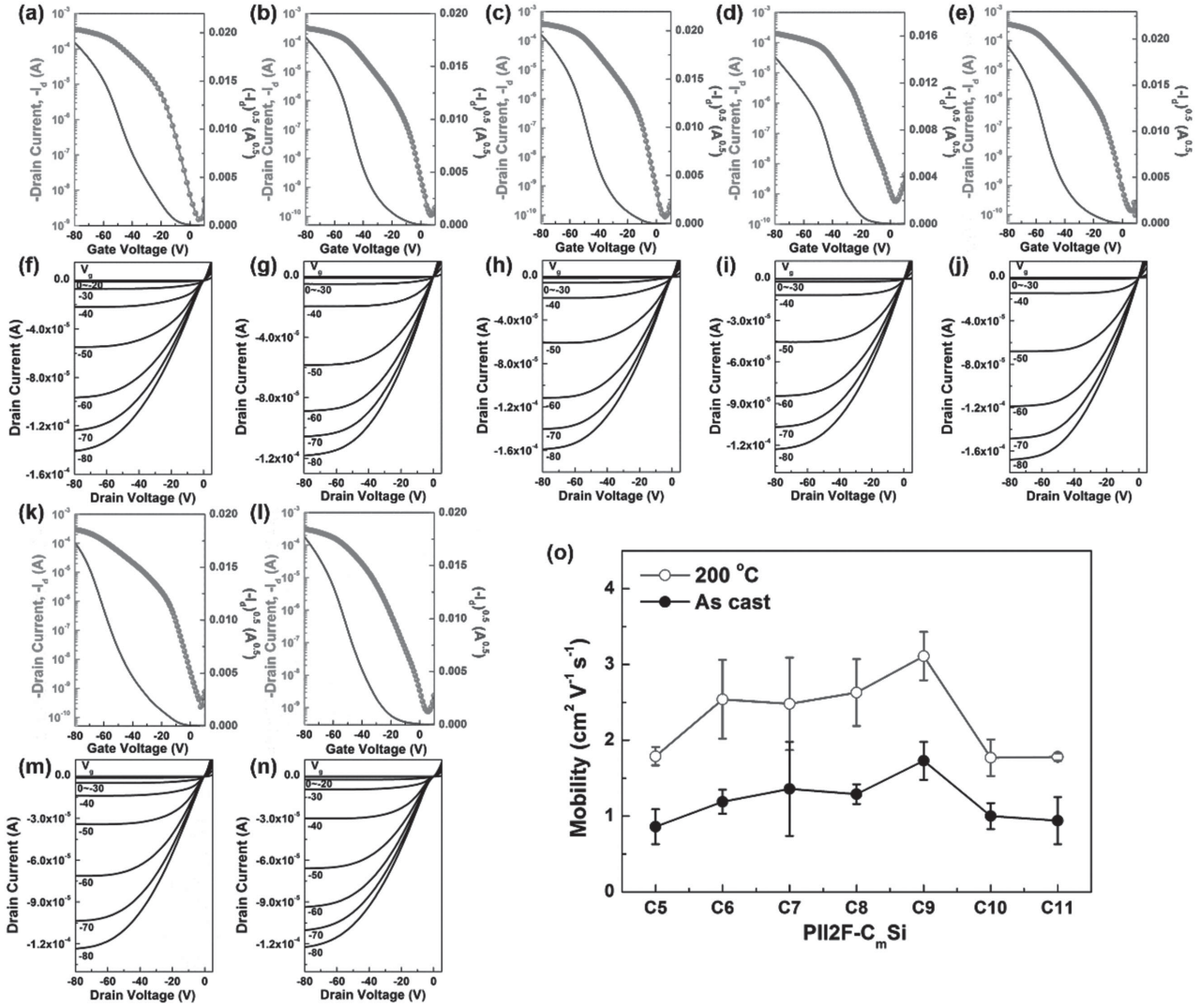

Figure 2. Transfer and output characteristics of transistors. a,f) PII2F-C_5Si, b,g) PII2F-C_6Si, c,h) PII2F-C_7Si, d,i) PII2F-C_8Si, e,j) PII2F-C_9Si, k,m) PII2F-C_{10}Si, and l,n) PII2F-C_{11}Si. o) Average mobilities for various PII2F-C_mSi-based devices. All the devices were annealed at 200 °C under nitrogen atmosphere for 1 h. The source-drain voltage was set to be −100 V for all measurements.

leads to increased π–π stacking distances, decreased crystalline domain coherent length, and increased face-on population, all are unfavorable to in-plane charge transport. On the other hand, increasing the spacer length above C9 further decreased π–π stacking distance and increased coherent length, which are expected to facilitate charge transport. However, at the same time, the crystallites became much less oriented out-of-plane, which is expected to hinder charge transport. The reason why spacer lengths lead to such morphological variations is unclear. We speculate that it may be related to the aggregation/crystallization dynamics during spin-coating. Longer, floppy side chains may slow down crystallization and offer more time for the polymer to assume thermodynamically favorable morphology, which is the edge-on orientation.

The highest mobility PII2F-C_9Si thin film, as fabricated from chloroform/chlorobenzene mix solvent, exhibited a π–π stacking distance of 3.39 Å, similar to that from the pure chloroform (Figure S5, Supporting Information). The in-plane FWHM of the chloroform/chlorobenzene-casted polymer film, however, had a smaller value (0.0725 $Å^{-1}$) than the chloroform-casted film of 0.0748 $Å^{-1}$. Interestingly, the π stacking distance for PII2F-C_9Si is smaller than PII2T-C_6Si (3.58 Å)[19] by 0.11 Å, which gave a mobility of 2.48 $cm^2\ V^{-1}\ s^{-1}$. PII2F-C_6Si also has a much smaller π–π stacking distance compared to PII2T-C_6Si. The π–π stacking distances for all PII2F-C_mSi are in the range of 3.38–3.41 Å, significantly smaller than most of high mobility semiconductors reported, such as PTDPPSe-SiC_m (≈3.6 Å),[20] IIDDT-C_m (3.57 Å),[22] and PII2T-Si (3.58 Å).[19] This is the synergistic result of choosing bifuran in polymer backbone and the use of the long linear alkyl-siloxane chain length (i.e., C11) as side chains, both of which lead to a denser molecular stacking between polymer chains. Meanwhile, the lamellar distance in this set of polymers remains below 28 Å, even though the branching point is 11 carbon away from the polymer

Table 2. OFET parameters of the studied polymers.

Polymer	As-cast				Annealed at 200 °C			
	μ_{max} [$cm^2\ V^{-1}\ s^{-1}$]	μ_{avg}[a)] [$cm^2\ V^{-1}\ s^{-1}$]	V_{th} [V]	I_{on}/I_{off} [–]	μ_{max} [$cm^2\ V^{-1}\ s^{-1}$]	μ_{avg}[a)] [$cm^2\ V^{-1}\ s^{-1}$]	V_{th} [V]	I_{on}/I_{off} [–]
PII2F-C_5Si	1.1	0.9 ± 0.2	−28 ± 2	≈10^5	1.9	1.8 ± 0.1	−21 ± 4	≈10^5
PII2F-C_6Si	1.3	1.2 ± 0.2	−36 ± 1	≈10^6	3.2	2.5 ± 0.5	−33 ± 3	≈10^6
PII2F-C_7Si	1.4	1.3 ± 0.6	−33 ± 6	≈10^6	3.2	2.5 ± 0.6	−29 ± 2	≈10^6
PII2F-C_8Si	1.4	1.3 ± 0.1	−39 ± 1	≈10^6	3.0	2.6 ± 0.4	−38 ± 7	≈10^6
PII2F-C_9Si	1.9	1.7 ± 0.3	−33 ± 3	≈10^6	3.4	3.1 ± 0.3	−35 ± 1	≈10^6
					(4.8)[b)]	(4.5 ± 0.2)[b)]	(−38 ± 3)[b)]	(≈10^6)[b)]
PII2F-C_{10}Si	1.2	1.0 ± 0.2	−36 ± 1	≈10^6	2.0	1.8 ± 0.2	−36 ± 3	≈10^5
PII2F-C_{11}Si	1.1	0.9 ± 0.3	−23 ± 1	≈10^6	1.8	1.8 ± 0.1	−27 ± 2	≈10^6
PII2F-Ref	0.1	0.1 ± 0.02	−12 ± 2	≈10^4	1.1	1.0 ± 0.2	−35 ± 3	≈10^5

[a)]The average mobilities of studied polymers from at least ten devices, and the error bars denote standard deviations; [b)]Devices were fabricated by chloroform/chlorobenzene (9/1, v/v) mix solution.

main chain. The molecular packing motifs with both face-on (lamellar spacing) and edge-on (π–π stacking) lead to fiber-like morphologies and outstanding charge carrier characteristics in PII2F-C_mSi polymer thin films.

The surface morphologies of polymer thin films were probed by using tapping mode atomic force microscopy (AFM) (**Figures 4** and S7, Supporting Information). The thin films of PII2F-C_mSi polymers exhibit nanofibrillar morphology with interconnected networks. This may also be an important factor for high mobility in these polymers as the formation of highly interconnected pathways between polymer chains is important for good charge carrier transport.[30] In contrast, this kind of fiber-like aggregates is absent in PII2F-Ref polymer thin film. Interestingly, clear terraces are found in PII2F-C_9Si thin film by a closer examination of images (Figure S6, Supporting Information), which was previously only observed with highly crystalline polymers with lamellar packing morphology, such as poly(2,5-bis(3-alkylthiophene-2-yl)thieno[3,2-*b*]thiophene) (PBTTT) polymer.[31] The terrace height measured via vertical sectional analysis is ≈26 Å. This value is close to that of GIXD measured out-of-plane lamellar spacing at 25.867 Å.

Table 3. Relevant crystallographic parameters for the studied polymer thin films.

Polymer	π–π spacing [Å]	In-plane FWHM [$Å^{-1}$]	Lamellar spacing [Å]
PII2F-C_5Si	3.413	0.0970	22.618
PII2F-C_6Si	3.402	0.0958	23.168
PII2F-C_7Si	3.414	0.0862	24.316
PII2F-C_8Si	3.393	0.0789	24.918
PII2F-C_9Si	3.392	0.0748	25.867
	(3.396)[a)]	(0.0725)[a)]	(26.049)[a)]
PII2F-C_{10}Si	3.392	0.0717	27.414
PII2F-C_{11}Si	3.379	0.0642	28.411
PII2F-Ref	3.637	n.a.	20.713

[a]The thin film was fabricated by chloroform/chlorobenzene (9/1, v/v) mix solution.

2.5. The Role of Side Chain Engineering in Donor–Acceptor Conjugated Polymers

The side chain engineering approach to move branching site away from conjugated backbone is becoming a common practice to improve charge transport and photovoltaic response in donor–acceptor conjugated polymers.[10,17–23] Currently, there are two major sets of solubilizing chains under investigation: branched alkyl chains and hybrid siloxane-containing chains. They both have advantages and disadvantages. The former is more commonly used and a great deal of experience has been accumulated to process such conjugated polymers. However, the synthesis of branched alkyl chains with different spacer lengths involves multiple-step synthetic efforts (typically more than five steps). In contrast, the synthesis of monomers with siloxane-containing side chains is straightforward and can be readily scaled up. The question here is that conjugated polymers with such side chains typically have limited solubility in high boiling point solvents such as chlorobenzene and dichlorobenzene. Interestingly, this feature enabled us to make pseudo-bilayered photovoltaics devices with PII2T-C_6Si and [6,6]-phenyl-C[71]-butyric acid methyl ester ($PC_{71}BM$) by systematically controlling the swelling and intermixing processes.[32] The side chains not only affect solubility and processability, but also have a profound influence on packing motifs. For instance, conjugated polymers with siloxane side chains have the tendency to simultaneously form face-on and edge-on orientations. Thus, it is critical to choose proper side chains in polymer design in order to achieve the desired properties for different applications.

3. Conclusion

We have prepared a series of isoindigo–bifuran polymers with alkyl-siloxane side chains, in which the length of linear alkyl spacer was systematically increased by one carbon atom at a time. Mobility as high as 4.8 $cm^2\ V^{-1}\ s^{-1}$ was obtained for PII2F-C_9Si, a value much higher than the previously reported

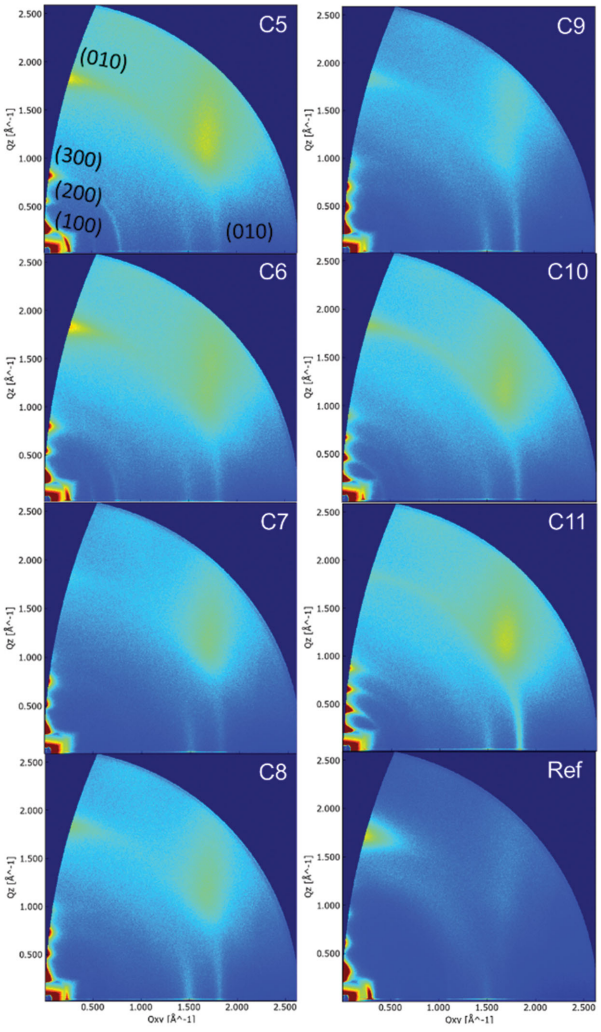

Figure 3. GIXD patterns of PII2F-C_mSi thin films, with m = 5–11 and PII2F-Ref thin film annealed at 200 °C. PII2F-Ref displays a face-on stacking structure. In contrast, PII2F-C_mSi films contain two kinds of textures, both face-on and edge-on packing planes were observed. All images are plotted using the same color scale.

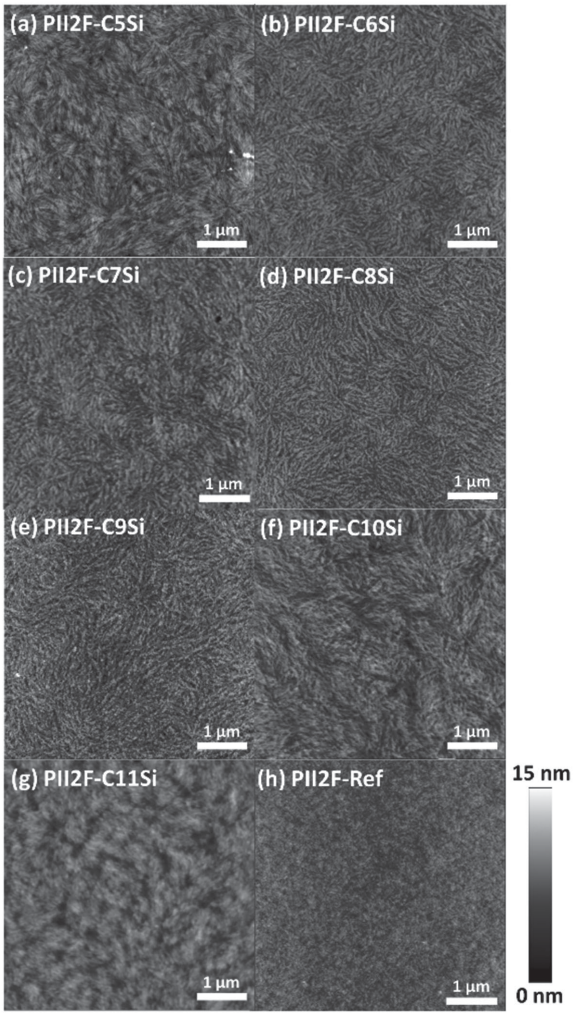

Figure 4. Tapping mode AFM topographies of spin-coated a–g) PII2F-C_mSi (m = 5-11) and h) PII2F-Ref thin film on OTS-treated Si wafer from chloroform solutions. All films were annealed at 200 °C for 1 h under a nitrogen atmosphere.

PII2T-C_6Si. The π–π stacking distances for this set of polymers are in the range of 3.38–3.41 Å, which are shorter than most other conjugated polymers. We concluded that it is important to move the branching point away from conjugated backbone in order to have efficient charge transport. When the branching point is at, or beyond, the third carbon from the conjugate backbone, the thin film charge transport characteristics do not change linearly with the length of the spacers. Other factors such as thin-film microstructure, crystallinity, domain size have a more significant impact on charge transport properties, and they can be rationally tuned by side chain engineering.

4. Experimental Section

General Method for N-Alkylation of 6,6-Dibromoisoindigo with n-Bromoalkene: To a suspension of 6,6′-dibromoisoindigo (10 mmol) and potassium carbonate (40 mmol) in dimethylformaldehyde (DMF) (50 mL), *n*-bromo-1-alkene (30 mmol) was added through a septum under an inert atmosphere at room temperature. The mixture was stirred for 10 h at 90–100 °C and then poured into methanol (200 mL). The precipitates were collected by vacuum filtration and successively washed by water and methanol. The obtained red solids were further purified by chromatography, eluting with methylene chloride and hexane (v:v = 1:2). The combined fraction was concentrated to dryness, then dissolved into hot chloroform, and finally precipitated into methanol, yielding red fine powders.

General Method for Hydrosilylation: To alkylated isoindigo (2.5 mmol) in anhydrous toluene (25 mL) was added 1,1,3,3,5,5,5-heptamethyltrisiloxane (5.2 mmol) under air, followed by addition of Karstedt catalyst (0.1 mmol%, divinyltetramethyl–siloxane platinum complex in xylene, 3 wt%). The reaction flask was capped and the mixture was stirred at 60 °C. The reaction was monitored by thin-layer chromatography (TLC) and stopped until the alkylated isoindigo was completely consumed. The obtained deep red solution was concentrated in vacuo and directly loaded onto silica gel column, eluted with methylene chloride and hexane (v:v = 1:2).

General Method for Polymerization: To a microwave vessel (35 mL, CEM Discover Automatic Microwave Reactor) charged with a string bar were added 5,5′-bis(trimethylstannyl)-2,2′-bithiophene (0.25 mmol) and

IID-C_nSi (0.25 mmol), $Pd_2(dba)_3$ (2 mol%), P(*o*-tyl)$_3$ (4 mol%), followed by the addition of degassed toluene (10 mL) under argon. The vessel was then sealed with a snap cap, purged with argon for 5–8 min, and immediately transferred to the microwave chamber. The polymerization conditions are listed as follows: power cycling mode; power, 250 W; power cycles, 200; temperature, 110–135 °C; heating, 120 s; cooling, 30 s; pressure, 150 psi; stirring, high. After the completion, the dark-blue mixture was suspended into acetone and the precipitates were collected by filtration through a Nylon membrane. The obtained solids were dissolved into hot chloroform. The strongly complexing ligand N,N-diethylphenylazothioformamide (CAS# 39484-81-6) was subsequently added (as a palladium scavenger). The polymer solution was concentrated and precipitated into acetone. The collected solids were filtered, washed with methanol and acetone, and dried at 60 °C under vacuum.

Fabrication and Characterization of Field-Effect Transistors: Highly n-doped Si wafers were used as substrates. A 300 nm thick SiO_2 layer (capacitance per unit area = 10 nF cm^{-2}) as a gate dielectric was thermally grown onto the Si substrates. The wafers were cleaned with compressed air and washed with toluene, acetone, and isopropanol in that order. The cleaned Si wafers were then modified with an octadecyltrimethoxysilane (OTS) self-assembled monolayer according to our reported method.[27] FET devices were deposited by spin coating from chloroform or chloroform/chlorobenzene (9/1; v/v) solution with a concentration of 4–5 mg mL^{-1} at a spin rate of 1000 rpm for 60 s. After drying, these samples were thermal annealed at 200 °C under nitrogen atmosphere. The top-contact source and drain electrodes were defined by 40 nm thick Au through a regular shadow mask, and the channel length (L) and width (W) were 50 and 1000 µm, respectively. FETs transfer and output characteristics were recorded in a N_2-filled glove box or under ambient by using a Keithley 4200 semiconductor parametric analyzer.

Supporting Information

Supporting Information is available from the Wiley Online Library or from the author.

Acknowledgements

J.M. and H.-C.W. contributed equally to this work. This work was supported by Air Force for Scientific Research (FA-5590-12-1-0190), National Science Foundation (Award No. DMR-1303178), the Department of Energy, Laboratory Directed Research and Development funding, under Contract DE-AC02-76SF00515. H.-C.W. thanks the Ministry of Science and Technology of Taiwan for financial support (MOST 102-2917-I-002-091).

Received: February 17, 2015
Revised: March 21, 2015
Published online: May 7, 2015

[1] H. Dong, X. Fu, J. Liu, Z. Wang, W. Hu, *Adv. Mater.* **2013**, *25*, 6158.
[2] H. Sirringhaus, *Adv. Mater.* **2014**, *26*, 1319.
[3] Y. Zhao, Y. Guo, Y. Liu, *Adv. Mater.* **2013**, *25*, 5372.
[4] S. Holliday, J. E. Donaghey, I. McCulloch, *Chem. Mater.* **2014**, *26*, 647.
[5] J. Mei, Y. Diao, A. L. Appleton, L. Fang, Z. Bao, *J. Am. Chem. Soc.* **2013**, *135*, 6724.
[6] H. Li, J. Mei, A. L. Ayzner, M. F. Toney, J. B. H. Tok, Z. Bao, *Org. Electron.* **2012**, *13*, 2450.
[7] M. Ikawa, T. Yamada, H. Matsui, H. Minemawari, J. y. Tsutsumi, Y. Horii, M. Chikamatsu, R. Azumi, R. Kumai, T. Hasegawa, *Nat. Commun.* **2012**, *3*, 1167.
[8] C. B. Nielsen, M. Turbiez, I. McCulloch, *Adv. Mater.* **2013**, *25*, 1859.
[9] I. Kang, H.-J. Yun, D. S. Chung, S.-K. Kwon, Y.-H. Kim, *J. Am. Chem. Soc.* **2013**, *135*, 14896.
[10] J. Mei, Z. Bao, *Chem. Mater.* **2014**, *26*, 604.
[11] T. Lei, J.-Y. Wang, J. Pei, *Chem. Mater.* **2014**, *26*, 594.
[12] C. B. Nielsen, I. McCulloch, *Prog. Polym. Sci.* **2013**, *38*, 2053.
[13] Z. Bao, A. Dodabalapur, A. J. Lovinger, *Appl. Phys. Lett.* **1996**, *69*, 4108.
[14] H.-J. Yun, J. Cho, D. S. Chung, Y.-H. Kim, S.-K. Kwon, *Macromolecules* **2014**, *47*, 7030.
[15] N. Rugen-Penkalla, M. Klapper, K. Müllen, *Macromolecules* **2012**, *45*, 2301.
[16] S. Chen, B. Sun, W. Hong, H. Aziz, Y. Meng, Y. Li, *J. Mater. Chem. C* **2014**, *2*, 2183.
[17] J.-H. Dou, Y.-Q. Zheng, T. Lei, S.-D. Zhang, Z. Wang, W.-B. Zhang, J.-Y. Wang, J. Pei, *Adv. Funct. Mater.* **2014**, *24*, 6270.
[18] J.-Y. Back, H. Yu, I. Song, I. Kang, H. Ahn, T. J. Shin, S.-K. Kwon, J. H. Oh, Y.-H. Kim, *Chem. Mater.* **2015**, *27*, 1732.
[19] J. Mei, D. H. Kim, A. L. Ayzner, M. F. Toney, Z. Bao, *J. Am. Chem. Soc.* **2011**, *133*, 20130.
[20] J. Lee, A. R. Han, J. Kim, Y. Kim, J. H. Oh, C. Yang, *J. Am. Chem. Soc.* **2012**, *134*, 20713.
[21] J. Lee, A. R. Han, H. Yu, T. J. Shin, C. Yang, J. H. Oh, *J. Am. Chem. Soc.* **2013**, *135*, 9540.
[22] T. Lei, J.-H. Dou, J. Pei, *Adv. Mater.* **2012**, *24*, 6457.
[23] I. Meager, R. S. Ashraf, S. Mollinger, B. C. Schroeder, H. Bronstein, D. Beatrup, M. S. Vezie, T. Kirchartz, A. Salleo, J. Nelson, I. McCulloch, *J. Am. Chem. Soc.* **2013**, *135*, 11537.
[24] A. T. Yiu, P. M. Beaujuge, O. P. Lee, C. H. Woo, M. F. Toney, J. M. J. Fréchet, *J. Am. Chem. Soc.* **2012**, *134*, 2180.
[25] M. S. Chen, O. P. Lee, J. R. Niskala, A. T. Yiu, C. J. Tassone, K. Schmidt, P. M. Beaujuge, S. S. Onishi, M. F. Toney, A. Zettl, J. M. J. Fréchet, *J. Am. Chem. Soc.* **2013**, *135*, 19229.
[26] A. Gandini, M. N. Belgacem, *Prog. Polym. Sci.* **1997**, *22*, 1203.
[27] Y. Zhou, T. Kurosawa, W. Ma, Y. Guo, L. Fang, K. Vandewal, Y. Diao, C. Wang, Q. Yan, J. Reinspach, J. Mei, A. L. Appleton, G. I. Koleilat, Y. Gao, S. C. B. Mannsfeld, A. Salleo, H. Ade, D. Zhao, Z. Bao, *Adv. Mater.* **2014**, *26*, 3767.
[28] Y. Ito, A. A. Virkar, S. Mannsfeld, J. H. Oh, M. Toney, J. Locklin, Z. Bao, *J. Am. Chem. Soc.* **2009**, *131*, 9396.
[29] Y. Huang, X. Guo, F. Liu, L. Huo, Y. Chen, T. P. Russell, C. C. Han, Y. Li, J. Hou, *Adv. Mater.* **2012**, *24*, 3383.
[30] R. Noriega, J. Rivnay, K. Vandewal, F. P. V. Koch, N. Stingelin, P. Smith, M. F. Toney, A. Salleo, *Nat. Mater.* **2013**, *12*, 1038.
[31] D. M. DeLongchamp, R. J. Kline, E. K. Lin, D. A. Fischer, L. J. Richter, L. A. Lucas, M. Heeney, I. McCulloch, J. E. Northrup, *Adv. Mater.* **2007**, *19*, 833.
[32] D. H. Kim, J. Mei, A. L. Ayzner, K. Schmidt, G. Giri, A. L. Appleton, M. F. Toney, Z. Bao, *Energy Environ. Sci.* **2014**, *7*, 1103.